International Journal of Heat and Mass Transfer 230 (2024) 125768

Contents lists available at ScienceDirect

International Journal of Heat and Mass Transfer

journal homepage: www.elsevier.com/locate/ijhmt

Experimental and modeling study on gasification of millimeter coal char particle via real-time measurement and correction of reaction temperature

Haigang Zhang [a,c], Zhongjie Shen [a,c,*], Jianliang Xu [a,c], Qinfeng Liang [a,c], Zhenghua Dai [a,b,c], Jianhong Gong [d], Haifeng Liu [a,c]

[a] National Energy Coal Gasification Technology Research and Development Center, East China University of Science and Technology, P. O. Box 272, Shanghai 200237, PR China
[b] School of Chemical Engineering and Technology, Xinjiang University, Urumchi 830046, PR China
[c] Shanghai Engineering Research Center of Coal Gasification, East China University of Science and Technology, P. O. Box 272, Shanghai 200237, PR China
[d] Sinopec Research Institute of Petroleum Processing, Beijing 100083, PR China

ARTICLE INFO

Keywords:
Coal gasification
Temperature distribution
Heat transfer
Ash layer
Modified kinetic model

ABSTRACT

Accurate measurement of particle temperature is crucial for calculating the kinetic parameters of gas-solid reaction, and predicting the carbon conversion in gasifiers. In this study, an in-situ experiment of single coal particle gasification was conducted by the online temperature measurement system. The heat and mass transfer processes of the internal carbon core were modeled under the consideration of the ash layer, and the actual reaction temperature of the internal core was calculated. The results showed a gradual decrease in particle surface temperature from the periphery to the interior during the gasification process. Highly non-uniform temperature distributions exceeding 80 K on the surface of the reacting particles were observed. Calculation results showed the temperature of the internal carbon core was lower than the surface by 27 K to 72 K from 1173 K to 1373 K. A modified kinetic model was proposed based on the unreacted core temperature and the reaction area. Compared with the traditional model, the proposed model prediction demonstrated a better agreement with the experimental data, particularly in the initial and late stages.

1. Introduction

With the implementation of the carbon-neutral policy in China, the energy industry, in which coal is the main resource, is facing tremendous pressure to reduce carbon emissions [1,2]. The clean and efficient utilization of coal has become an urgent task. In the field of the coal chemical industry, gasification technology plays a vital role in the conversion of coal into clean energy and the reduction of carbon emissions [3,4]. During the gasification process, the coal particles react rapidly with the reaction gas in the furnace under a high-temperature environment, and the particle size, coal type, and pore structure of coal char have a significant impact on the gasification activity, affecting the conversion of the residual carbon [5–7]. Hence, it is meaningful to explore methods for enhancing gasification efficiency and minimizing carbon content in the form of residue in fine slag, as this is a critical aspect of gasification process research.

For gas-solid reactions occurring at high temperatures, such as gasification or combustion, exhibit rapid reaction rates that are sensitive to temperature variation, and the conversion heavily relies on the temperature of the particles involved [8,9]. Accurate temperature measurements for particles are essential for enhancing the energy conversion and efficiency of fuels [10,11]. Meanwhile, in reactions with notable thermal effects, variations in reaction rates at the particle surface also led to inhomogeneities in the surface temperature distribution [12,13]. For instance, in the gasification process, differences in surface temperature among particles contribute to non-uniform Stefan flow, introducing additional forces that impact the balance of particulate forces during high-temperature reaction processes [14,15]. This, in turn, affects the dispersion and reaction of particles within the fluidized bed gasifier [16].

Previous studies including simulations for large-scale systems of gasification ignored the local temperature difference of the particle and instead relied on the reactor temperature as the average particle temperature for further calculation, but a certain deviation from the actual temperature still existed, affecting the calculation accuracy [17,18]. Küster et al. [13] revealed that inhomogeneous particles affect gasification kinetics, and for reactive particles, there was a significant

* Corresponding author.
E-mail address: zjshen@ecust.edu.cn (Z. Shen).

https://doi.org/10.1016/j.ijheatmasstransfer.2024.125768
Received 19 March 2024; Received in revised form 22 May 2024; Accepted 23 May 2024
Available online 31 May 2024

Nomenclature

A	Correction parameter
$A_{p,t}$	Heat transfer area at time t (m^2)
B	Correction parameter
Bi_m	Biot number
C	Infrared thermal camera parameter
C_C	Carbon concentration ($mol \cdot m^{-3}$)
C_{CO2}	Gas phase concentration ($mol \cdot m^{-3}$)
C_p	Specific heat capacity ($J \cdot g^{-1} \cdot K^{-1}$)
d	particle diameter (m)
D_e	Effective diffusion coefficient ($m^2 \cdot s^{-1}$)
D_m	Molecular diffusion coefficient ($m^2 \cdot s^{-1}$)
D_n	Knudsen diffusion coefficient ($m^2 \cdot s^{-1}$)
E	Activation energy ($J \cdot mol^{-1}$)
$F(x)$	Structural factor
h_g	Convection coefficient ($W \cdot m^{-2}\ k^{-1}$)
k_0	Pre-exponential factor (s^{-1})
k_c	Reaction rate constant (s^{-1})
L	Total radiant intensity (W/m^2)
m	Thermometric equation parameter
M_{CO2}	Molar mass of carbon ($g \cdot mol^{-1}$)
m_t	Particle mass at time t ($g \cdot mol^{-1}$)
n	Thermometric equation parameter
Q_c	Particle heat absorption ($J \cdot s^{-1}$)
$Q_{c,c}$	Carbon core heat absorption ($J \cdot s^{-1}$)
$Q_{c,t}$	Reaction heat of carbon core ($J \cdot s^{-1}$)
$Q_{c,d}$	Carbon core heat conduction ($J \cdot s^{-1}$)
Q_d	Heat conduction ($J \cdot s^{-1}$)
Q_h	Convective heat transfer ($J \cdot s^{-1}$)
Q_r	Radiative heat transfer ($J \cdot s^{-1}$)
Q_t	Reaction heat ($J \cdot s^{-1}$)
R	Molecular gas constant ($J \cdot mol^{-1} \cdot K^{-1}$)
r_{CO2}	Gas reaction rate ($mol \cdot m^{-3} \cdot s^{-1}$)
r_c	Carbon consumption rate ($mol \cdot m^{-3} \cdot s^{-1}$)
$R_{p,t}$	Particle radius (m)
r_{pores}	Average pore size (m)
S_t	Reaction area at time t (m^2)
T_0	True temperature of the particle(K)
$T_{a,t}$	Ash layer temperature at time t (K)
T_e	Environmental temperature (K)
T_r	Measured radiation temperature (K)
T_t	Carbon temperature at time t (K)
$T_{t\text{-}0.2}$	Carbon temperature at time t-0.2 (K)
T_w	Heating crucible temperature (K)
x	Conversion rate

Greek symbols

ΔH	Gasification enthalpy ($J \cdot mol^{-1}$)
ε	Porosity
ε_r	Emissivity
λ	Infrared wavelength (nm)
λ_s	Ash layer thermal conductivity ($W \cdot m^{-1} \cdot k^{-1}$)
τ	Tortuosity factor
τ_b	Optical transmittance
η	Effectiveness factor
φ_c	Fixed carbon content
Φ	Modified Thiele modulus
σ	Standard deviation
ψ	Pore structure parameter in RPM

Subscripts

0	Initial moment of reaction
g	Gas
m	Ash and carbon mixtures
p	Particle
s	Ash layer
t	Reaction time
w	Inner wall
0.2	Time step

difference between the gas and particle temperature (ΔT≈40 K at 1293 K, lignite). Sładek's [19] study also confirmed this result and established a function to correlate the mean particle temperature with its temperature variance, which can be used in numerical modeling to include the influence of varying reactivity for individual particles. Due to the limitation of the particle size and reaction environment, it is challenging to directly obtain the actual temperature distribution on the particle surface, especially for the high temperature (>1000 K) reactions [20,21]. Accordingly, it is necessary to realize the measurement of particle temperature at high temperatures by establishing a micro-infrared thermometry platform.

The development of mathematical models to describe coal gasification processes is a crucial aspect of studying gasification and provides a theoretical foundation for achieving efficient conversion of the fluidized bed gasification technology [22,23]. A variety of models were proposed early, including the volume model (VM), grain model (GM), and the random pores model (RPM) [24–26]. Among these models, modified RPM is commonly used to describe the whole coal-char gasification process and incorporates pore structure parameters to explain the occurrence of rate peaks during the gasification process [27,28]. He et al. [29] applied the random pore model to fit and predict different coal char gasification reactivities with a high fitting degree, and structural factors were incorporated to elucidate the impact of ash on pore properties during gasification. However, the RPM model does not account for the temperature distribution within the reaction layer, which is influenced by particle size, nor does it consider the effects of the ash layer on the heat and mass transfer processes. In gasifiers, the thermal behavior inside char particles varies with particle size, as larger particles transfer heat over longer distances and possess larger reaction areas [30]. However, there is limited literature discussing the effect of the ash layer on the reaction heat and mass transfer [31,32].

For gasification at medium temperatures (900–1100 °C) in the fluidized bed gasifier, temperature is a critical parameter that influences the local reactivity of particles and the overall conversion. Previous studies and mathematical models of coal gasification processes have paid insufficient attention to the local temperature difference of particles and the temperature effect. Therefore, an in-situ experiment of single coal particle gasification was conducted by the online temperature measurement system to measure the temperature variation on the particle surface in real-time, which allows for the assessment of the local reactivity difference. Considering the presence of the ash layer, the actual reaction temperature of the internal core was calculated. This work aims at a gasifier operating at atmospheric pressure, and the experimental and modeling results are consistent with the heat and mass transfer process and provide a reference for predicting and modeling the reactivity of industrial fluidized bed gasifiers.

2. Materials and methods

2.1. Materials

The experimental raw material used in this study was Yili coal (Xinjiang, China). After drying, the coal was crushed and screened to obtain different particle size ranges. The coal samples with a particle size

of 0.8–1.2 mm were selected as the raw material for gasification in this experiment, and the weight of a single particle was about 0.6–1.0 mg. The proximate and ultimate analyses of the samples were carried out on a 5E-MACIII (Kaiyuan company, China) and a Vario MACRO element analyzer (Elementar, Germany), the results are shown in Table 1. The ultimate analysis results are based on the combustible part, the element contents of C, H, S, and N can be directly measured, and the oxygen content was obtained by difference. The fusion temperature (FT) of coal ash under the CO/CO_2 atmosphere was 1607 K measured by the 5E-AF4000 ash fusion point tester (Kaiyuan, China).

2.2. In-situ temperature measurement

To facilitate the observation and recording of the reaction process, an infrared temperature measurement device (FLIR A615, America) combined with a hot stage (Linkman, Britain) was constructed, as illustrated in Fig. 1. The details of the hot stage used in this study were introduced in our previous study [33]. In this study, micron-scale particles of bituminous coal char were selected for gasification experiments, and the experiments were conducted at temperatures ranging from 900 to 1100 °C and under ordinary pressure, which are consistent with the operating conditions of current major fluidized bed gasifier technology, including U-Gas ash fusion agglomeration gasification, KBR transport gasifier, ordinary pressure circulating fluidized bed technology (CFBR), and staged fluidized bed gasifier [34]. As shown in Fig. 1, the temperature of the hot stage was measured by two thermocouples placed outside and inside the heated crucible. The thermocouples were named TC1 and TC2, respectively. These thermocouples measured the temperatures at the edge and the center of the heated crucible respectively to verify the accuracy of the temperature field determined by the infrared camera measurements. The gasification experiments were conducted within the high-temperature hot stage, where the sample was brought to a set temperature at a ramp rate of 25 K/min, while the infrared camera was utilized to record the temperature distribution of particles during the gasification process through the visualization window located on the top of the hot stage. Meanwhile, the conversion curves for individual particle at set temperatures were obtained by recording the weight loss. The experimental heat absorption curves were obtained by the thermogravimetric and differential scanning calorimetry (STA449-F3, Netzsch, German).

The FLIR A615 infrared camera is equipped with an uncooled vanadium oxide detector, which generates a high thermal image of 640*480 pixels in the long infrared wavelength band (7.5–14 μm). To observe millimeter-sized particles within the hot stage chamber, a 1.5x close-up lens with a resolution of 25 μm was used in this study. According to the test results of the camera temperature measurement, the test repeatability error is ±2 K in the temperature range of 573~2273 K, which proves the device has a high measurement accuracy.

In the experiment, the total infrared radiation of the coal particle entering the infrared thermal camera included the real object radiation and the environmental infrared radiation reflection. Thus, the total radiation intensity can be expressed as Eq. (1).

$$L = \tau_b \cdot \varepsilon_r \cdot L(T_0) + \tau_b \cdot (1 - \varepsilon_r) \cdot L(T_e) \tag{1}$$

where L is the total radiation intensity; τ_b is the optical transmission transmittance; ε_r is the sample emissivity; T_e is the environmental temperature outside the heating crucible; T_0 is the true temperature.

Table 1
Proximate and ultimate analyses of Yili coal.

Proximate analysis (ad, wt. %)			Ultimate analysis (daf, wt. %)				
Moisture	Combustible part	Ash	Combustible part				
			C	H	S	N	O*
6.23	84.14	9.63	81.66	4.28	1.57	1.33	11.15

* The oxygen content was obtained by difference.

According to the previous study [35], in the 7.5–14 mm band, based on Planck's law, the radiated power can be written approximately as Eq. (2).

$$L_R(T_0) = \int_{\Delta\lambda} L_\lambda(T_0) d\lambda \approx C T_0^{1/n} \tag{2}$$

where $\Delta\lambda$ is the wavelength range received by the camera, C and n are the parameters related to the spectral bands received by the infrared thermal camera.

The deviation of the measured temperatures relied on the radiation intensity. As shown in Fig. 1, in the experiment conducted in the hot stage, the samples were placed in the center of the heated crucible with an inner diameter of 5 mm, and the environmental temperature except for the heated crucible was approximated as consistent with room temperature (298 K). For the high-temperature particle (>1000 K), the true radiation received from the sample is much higher than the environmental radiation outside the heated crucible by two orders of magnitude. Hence, the effect of environmental radiation on the temperature measurement results is neglected here, as shown by the Stefan-Boltzmann law. Further, the logarithmic equation between the measured temperature (T_r) and the true temperature (T_0) can be described as Eq. (3) after considering the external optical transmittance (τ_b).

$$\ln\left(\frac{T_r}{T_0}\right) = m \cdot \ln(\varepsilon_r) + n \cdot \ln(\tau_b) \tag{3}$$

The relationship between the real temperature and the radiant temperature can also be written as Eq. (4).

$$T_0 = \frac{T_r}{\varepsilon_r^m \cdot \tau_b^n} \tag{4}$$

where m and n are the function parameters. $m = 1.91$ $n = 1.93$, the equipment calibration and parameterization of equations including emissivity and transmittance can be found in the Supplementary Materials.

3. Mass and heat transfer analysis

3.1. Gasification process analysis

The coal gasification experiment was carried out at a temperature lower than the ash melting point, and the carbon core was continuously consumed and shrank throughout the reaction process. Simultaneously, the ash layer presented on the surface of the coal char gradually became exposed, resulting in the formation of a compact and porous layer without partial melting or collapsing. This shrinkage phenomenon is shown in Fig. 2, and the projected area of the particle decreased by approximately 17 % before and after the complete reaction.

The presence of the ash layer hindered the gas-solid contact and heat transfer. Therefore, to evaluate the effect of the ash layer on the chemical reaction and heat transfer process of the unreacted carbon core, assumptions were given as follows before further analysis.

(1) Coal char has a uniform density and diffusivity during gasification.
(2) Ash is uniformly distributed in the coal particle.
(3) Variation of ash shell volume was neglected during the reaction.
(4) No reaction between minerals in the ash and carbon.

3.2. Mass transfer and kinetics model modification

Coal gasification is a typical gas-solid reaction, and the coal gasification experiments were carried out in the pure CO_2 atmosphere. During

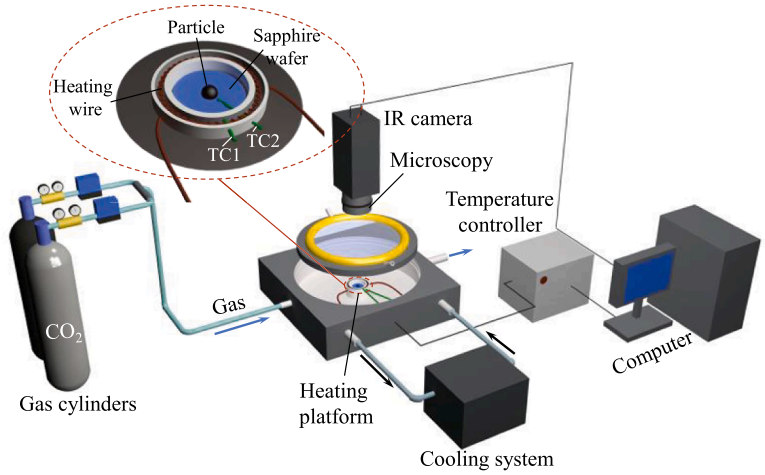

Fig. 1. Schematic diagram of the online temperature measurement system.

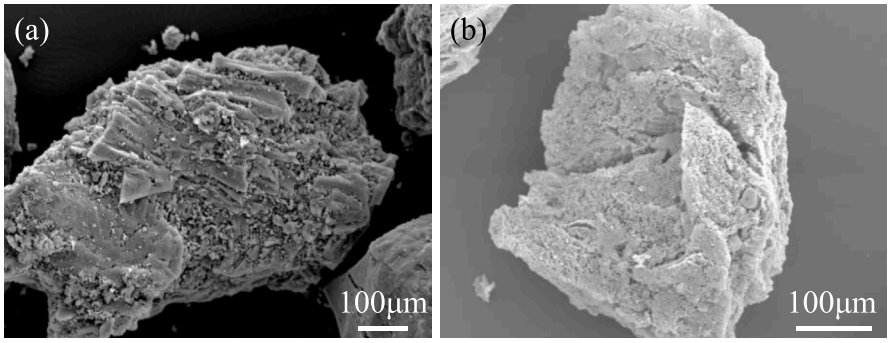

Fig. 2. The morphology of coal particle (a) and ash particle after complete gasification (b).

gasification, a single coal char was assumed as a sphere with a radius R_p. The carbon could be completely converted in the reaction stages and the gasification was regarded as a first-order reaction and the reaction rate can be expressed as a function of temperature and conversion.

$$C + CO_2 \xrightarrow{k_c} 2CO, \Delta H = 173.4 kJ / mol \tag{5}$$

The reaction takes place at the interface between gas-solid phases of the coal char. From a macroscopic perspective, the intrinsic reaction rate can be expressed as Eq. (6)

$$r_{CO_2} = k_c \cdot St \cdot C_{CO_2} \tag{6}$$

$$k_c = k_0 \cdot \exp\left(-\frac{E}{RT}\right) \tag{7}$$

Microscopically, the gasification process consists of gas diffusion (external and internal), adsorption, reaction, and desorption process, the slowest step dictates the overall reaction rate. Hence, the mass transfer equation of the gas-phase process based on the equilibrium relationship between CO_2 consumption, mass transfer of internal diffusion, and the reaction was obtained as Eq. (8).

$$\varepsilon \frac{\partial CCO_2}{\partial t} = \frac{D_e}{R_{p,t}^2} \cdot \frac{\partial}{\partial R}\left(R_{p,t}^2 \frac{\partial CCO_2}{\partial R}\right) + r_{CO_2} \tag{8}$$

where, boundary condition: $R=R_0$, $C_{CO2}=4.21 \times 10^{-4}$ g/cm^3.

Conservation of carbon consumption and reaction:

$$-\frac{\partial C_c}{\partial t} = r_c \tag{9}$$

Under experimental conditions, the injected gas was in a laminar flow state with a low Reynolds number (Re < 200). Based on Eq. (10), the mass transfer Biot number could be calculated at about 5 ($Bi_m \approx 5 > 1$), inducting the mass transfer time of gas inside the particle is higher than that outside the particle. The effect of external diffusion resistance on the concentration distribution of particles could be neglected.

$$Bi_m = \frac{t_{Di}}{t_{De}} = \frac{k_c \cdot R_0}{D_e} \tag{10}$$

In Eq. (10), the CO_2 effective diffusion coefficient (D_e) inside the particles includes the volumetric diffusion and the Knudsen diffusion of the gas in the pores [36], which is expressed as:

$$D_e = \frac{\varepsilon}{\tau}\left(\frac{1}{D_n} + \frac{1}{Dm}\right)^{-1} \tag{11}$$

$$D_n = \frac{2}{3}\bar{r}_{pores}\sqrt{\frac{8RT}{\pi MCO_2 \times 10^{-3}}} = 9.70 \times 10^3 \cdot \bar{r}_{pores} \cdot \sqrt{\frac{T}{MCO_2}} \tag{12}$$

$$D_m = 1.39 \times 10^{-1} \cdot (T/273.2)^{1.75} \tag{13}$$

On the reaction surface of the coal char particle, the deceleration step of the gasification could be determined based on the modified Thiele modulus [37].

$$\Phi = \frac{R}{3} \cdot \sqrt{\frac{k_c}{D_e}} \tag{14}$$

Hence, the effectiveness factor could be calculated based on Eq. (15).

$$\eta = \frac{1}{\Phi}\left(\frac{1}{\tanh(3\Phi)} - \frac{1}{3\Phi}\right) \tag{15}$$

At temperatures ranging from 1173 to 1373 K, $\Phi \approx 0.062 < 1$, $\eta > 0.9$, The intrinsic chemical reaction rate is slower than the internal diffusion. Therefore, the effect of mass transfer on the gasification can be neglected, and the gasification was in the chemical reaction control regime within the temperature range. The rates of gas consumption, carbon consumption, and reaction are equivalent.

$$r = r_c = r_{CO_2} \tag{16}$$

Meanwhile, in the gasification process, the specific surface area of the char involved in the gasification was changed. Hence, an eigenfunction, the structure factor $F(x)$, was introduced to describe the variation, and a Taylor expansion of $F(x)$ at $x = 1$ was carried out based on the boundary conditions.

$$S_t = S_0 \cdot F(x) \tag{17}$$

$$F(x) = \mathrm{A}\cdot(1-x) + \mathrm{B}\cdot(1-x)^2 + R(x) \tag{18}$$

Based on the boundary conditions: F(0) = 1, F(1) = 0, we got the relationship of the parameters of A and B, A+B = 1.

As a result, a modified mathematical model for single particle conversion and reaction rate in the gasification process was obtained by combined Eqs. (6), (9) and (16) ~ (18):

$$\frac{\partial x_c}{\partial t} = k_C \cdot S_0 \cdot \frac{C_{CO_2}}{C_c} \cdot (1-x) \cdot (1 - \mathrm{B}x) \tag{19}$$

$$x = 1 - \frac{1-\mathrm{B}}{\exp\left((1-\mathrm{B})\cdot k_C \cdot S_0 \cdot \frac{C_{CO_2}}{C_c} t\right) - \mathrm{B}} \tag{20}$$

Meanwhile, volume model (VM), grain model (GM), and random pore model (RPM) could also describe the gasification process, which is summarized in Table 2. The conversion equation *vs.* t is also listed in Table 2, whereas the activation energy and pre-exponential factor were obtained by fitting the experimental results

3.3. Heat transfer analysis

As the carbon consumed rate is higher on the external surface of the particle compared to the interior, and the carbonaceous layer on the particle surface is first consumed to form an ash layer, followed by the internal part. Therefore, in this study, to describe the process, the particle during the reaction is assumed to be a carbonaceous core that continues to react. The exposed ash layer hindered the heat transfer between the reaction interface and the gas phase, and the schematic diagram of the heat transfer process during gasification is displayed in Fig. 3. The schematic from left to right indicates the deepening of the reaction.

Table 2
Summary of conversion equation of gasification models.

Model	Assumption	Conversion equation
This study	Unreacted core encased in a porous ash layer	$x = 1 - \frac{1-\mathrm{B}}{\exp\left((1-\mathrm{B})\cdot k_C \cdot S_0 \cdot \frac{C_{CO_2}}{C_c} t\right) - \mathrm{B}}$
VM [29]	Homogeneous reaction of solid reactant	$x_{VM} = 1 - \exp(-kt)$
GM [29]	Surface reaction on the nonporous grains	$x_{GM} = 1 - \left(1 - \frac{1}{3}kt\right)^3$
RPM [38]	Independent and growth pores	$x_{RPM} = = 1 - \exp\left[-kt\left(\frac{\psi kt}{4} + 1\right)\right]$

In a single particle gasification at constant temperature, the energy balance included the gasification heat (Q_t), heat radiation with the environment (Q_r), convective heat transfer with the gas (Q_h), and particle heat absorption (Q_c). The total energy balance equation could be expressed as Eq. (21).

$$Q_t = Q_r + Q_c + Q_h \tag{21}$$

For the unreacted carbon core inside the particle, the energy balance could be further simplified as Eq. (22) based on the known temperature of the ash layer. The total gasification heat was carbon core heat absorption ($Q_{c,c}$), and heat conduction with the ash layer ($Q_{d,c}$). Values of model parameters used in this study were given in Table 3.

$$Q_{c,t} = Q_{c.c} + Q_{c,d} \tag{22}$$

The gasification heat could be expressed as:

$$Q_{c,t} = \frac{\varphi_c \cdot \Delta m_t \cdot \Delta \mathrm{H}}{\mathrm{M}_C} \tag{23}$$

$$\Delta m_t = m_0 \cdot \Delta x_t \tag{24}$$

For the spherical char particle, the heat transfer area was calculated as:

$$A_{p,t} = 4\pi R_{p,t}^2 = A_{p,0} \cdot (1 - x_t)^{2/3} \tag{25}$$

The unreacted carbon core heat absorption could be expressed as:

$$Q_{c,c} = C_p \cdot \varphi_c \cdot \Delta m_t \cdot (T_t - T_{t-0.2}) \tag{26}$$

where the time step selected was 0.2 s in this study.

The heat conduction between the ash layer and the unreacted carbon core could be expressed as:

$$Q_{c,d} = -\lambda_s \cdot A_{p,t} \cdot \frac{\partial T}{\partial R} = -\lambda \cdot A_0 \cdot (1 - x_t)^{2/3} \cdot \frac{T_t - T_{a,t}}{R_0 \cdot x_t^{1/3}} \tag{27}$$

The thermal equilibrium of the particles when controlled by the reaction rate can be further derived:

$$\frac{m_0(1-\varphi)\cdot \Delta x_t \cdot \Delta \mathrm{H}}{\mathrm{M}_C} = -\lambda \cdot A_0 \cdot (1 - x_t)^{2/3} \cdot \frac{T_t - T_{a,t}}{R_0 \cdot x_t^{1/3}} + C_p \cdot m_0 \cdot \Delta x_t \cdot (T_t - T_{t-0.2}) \tag{28}$$

4. Results and discussion

4.1. Conversion and reactivity

The weight loss and conversion results of a single coal particle during gasification processes are shown in Fig. 4. The volatiles and moisture have been released during the heating process, and the weight loss variation of the coal particle in the constant temperature reaction stage is the gasification of fixed carbon, as shown in Fig. 4(a). The initial reaction time is when CO2 starts to be injected. The gasification conversion curves and reaction rates in the constant temperature sections of 1173 K, 1273 K, and 1373 K are shown in Fig. 4(b) and (c). The trend of the coal-char particle conversion curves at different temperatures was similar, with a rapid near-linear increase in the first and middle stages of the reaction and a gradual increase in the late stages. In the experimental temperature range, the temperature had a significant effect on the gasification reactivity of coal particles. For the gasification of a single-particle, the average reaction rate at 1373 K and 1273 K with a carbon conversion of 0.9 ($x = 0.9$) was 6.4 and 3.0 times higher than that at 1173 K, respectively. Besides, the linear relationship between $\ln(r_c)$ and $1/T$ indicated the direct impact of temperature on the gasification reactivity, and it also confirmed that the gasification was in the intrinsic kinetic control region during the experimental conditions.

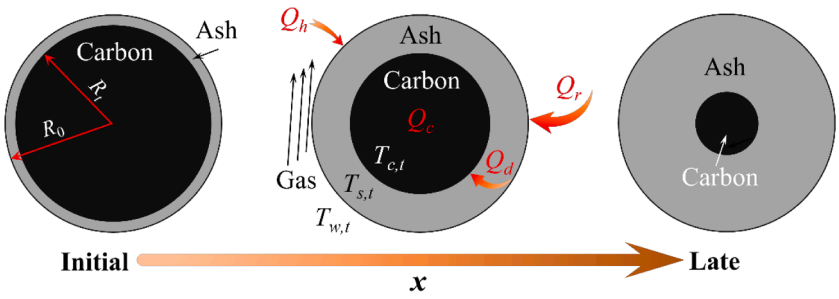

Fig. 3. Schematic diagram of heat transfer and conversion in single particle gasification process.

Table 3
Values of the heat and mass transfer parameters used in this study [38–40].

Parameter	Value	Parameter	Value
C_p (J·g^{-1}·K^{-1})	1.2	r_{pores} (nm)	25.33
C_c (g/cm^3)	0.428	R_0 (m)	5.0×10^{-4}
C_{CO2} (g/cm^3)	4.21×10^{-4}	σ (W·m^{-2}·K^{-4})	5.67×10^{-8}
D_e (cm^2/s)	2.39×10^{-4}	Φ	0.096
k_c (s^{-1})	3.25×10^{-3}	τ	4
m_0 (g)	6.08×10^{-4}	E (%)	0.77
M_c (g·mol^{-1})	12	λ_s (W·m^{-1}·K^{-1})	0.23

4.2. Particle surface temperature distribution

Fig 5. shows the surface temperature distribution (STD) at the lowest average particle temperature during gasification. In Fig. 5, according to the previous method in Supplementary Materials, a 500*500 μm rectangular area at the center of the particle was selected and the surface temperature distribution in this area was measured. The temperature points located at the periphery of the sample were omitted from the analysis. This decision was made to ensure the accuracy and reliability of the temperature measurements, as the edge of the sample is particularly susceptible to external heat sources [19].

Overall, the temperature of the central region of the coal particle surface exhibited a lower value compared to its surroundings, showing a layered decrease from the outer periphery towards the center. The result proved the cascade of char particle gasification, which is consistent with the assumption of an unreacted carbon core. The external carbon had completed the reaction, and the temperature of the peripheral surface was approaching the ambient temperature. The size of the central low-temperature region exhibited an inverse relationship with the reaction temperature. Specifically, at a temperature of 1173 K, the surrounding temperature was high and the central low-temperature region was small; while, at 1373 K, the central low-temperature region is larger and the temperature is relatively lower. As the gasification temperature increased, the difference between the particle center temperature and the ambient temperature gradually amplified. Influenced by the surface structure and mineral distribution of coal char, the surface gasification characteristics of coal char were different, resulting in uneven surface temperature distribution of particles at the same gasification temperature. Under experimental conditions, the surface temperature difference could be up to 80 K. The coal particle exhibited high gasification activity and rapid gasification rates at the low-temperature point.

Influenced by the coal particle structure and the variability of surface ash, the surface temperature distribution between different particles was different. Hence, the gasification experiments were repeated five times for each group of experimental conditions, and the repeatability measurements of the temperature difference in the gasification process of coal char particles surface are shown in Table 4. With the increment of the ambient temperature, the mean value of the maximum temperature difference ($\Delta\overline{T}_{0,max}$) was increased, and the thermal effect was more obvious, which was related to the reactivity. Meanwhile, statistical analysis of various particles shows the standard deviation (σ) of the maximum temperature difference decreased with the increase in temperature. The measurement deviation is acceptable and does not affect further analysis of the gasification heat transfer process, as the maximum temperature difference ($\Delta\overline{T}_{0,max}$) due to the thermal effect is higher than the measurement deviation. Additionally, it was found that at higher temperatures, the standard deviation of the temperature difference decreased, indicating that the inhomogeneity of the feedstock at higher temperatures has less effect on the overall temperature variability of the particles, which is attributed to the high reactivity of the particles at higher temperatures.

4.3. Temperature variation in gasification

Fig. 6(a)~(c) illustrates the variation of the measured average temperature of the ash layer surface during gasification at different temperatures. During the gasification process, the internal carbon core

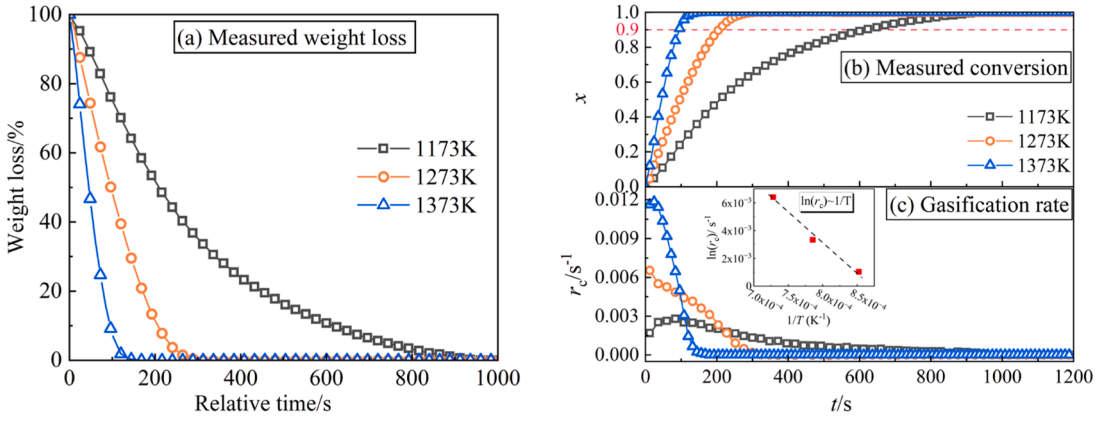

Fig. 4. Measured weight loss (a), conversion curves (b), and gasification rate (c) of coal particle during gasification at different temperatures.

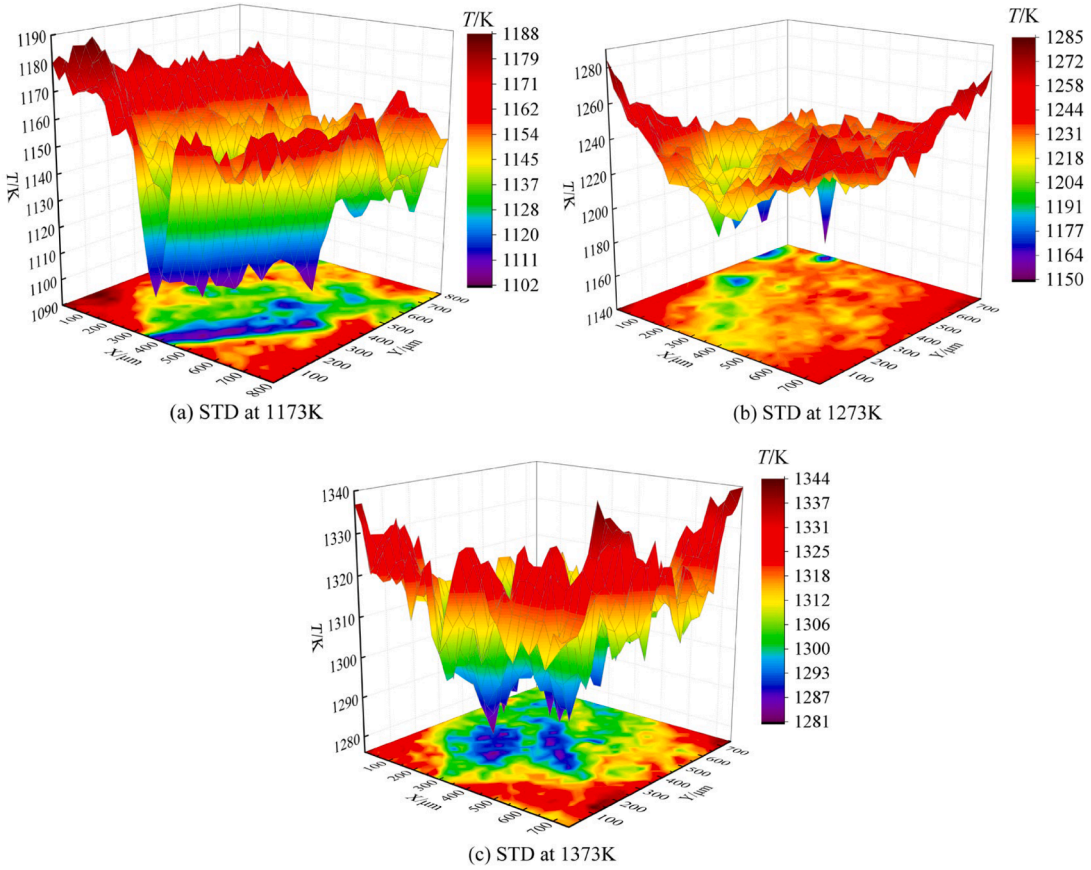

(a) STD at 1173K

(b) STD at 1273K

(c) STD at 1373K

Fig. 5. Surface temperature distribution (STD) at different reaction temperatures of coal char at the lowest particle temperature during gasification.

Table 4
Volatility analysis of average temperature measurements during gasification.

T_w/K	$\Delta\overline{T}_{0,max}$/K	σ/K
1173	15	10
1273	29	7
1373	54	5

shrank and the ash layer was exposed on the surface of the coal char. The experimental temperature measurement results by the online temperature measurement system were the temperature of the exposed ash layer on the surface of coal char. As the reaction proceeded, the difference in the average temperature of the particle surface initially increased and then decreased. This trend was associated with the gradual decrease in the gasification rate. The return to ambient temperature slightly lagged behind the overall reaction time. Additionally, the reactivity of coal char gasification was significantly influenced by temperature. With the increase of gasification temperature, the temperature variation curve shifted from a through to a sharp peak. The average temperature difference on the particle surface, referring to the difference with the equipment temperature, increased, and the maximum average temperature difference was increased from 17 K to 56 K when the gasification temperature was increased from 1173 K to 1373 K, respectively. Simultaneously, the relative time (τ_t=t_t/t_{total}) at which the lowest temperature point occurred was observed to be skewed with the increasing reaction temperature. This phenomenon arises due to the rapid rise in reaction rate, causing a slight delay in the heat transfer rate to the surface of the ash layer.

The reaction rate is highly dependent on the temperature. To obtain accurate kinetic data, it is crucial to determine the actual gasification temperature of the unreacted carbon core. The actual gasification temperature of the unreacted core inside the particle could be calculated by Eq. (28), and the results are shown as the red line in Fig. 6(a)~(c). Throughout the reaction, the temperature variation in the unreacted carbon core is correlated with the reaction rate and exhibits a distinct difference lower than the temperature change in the ash layer. Notably, the temperature of the unreacted carbon core reaches its minimum point in the middle stage of the reaction, regardless of the reaction temperature.

The results of the maximum temperature difference during the reaction process are shown in Fig. 6(d), the temperature difference between the unreacted carbon core reached 45 K, 59 K, and 128 K at 1173 K, 1273 K, and 1373 K, respectively. Compared with the previous results [41,42], the temperature difference between the unreacted carbon core and the environment was higher than the measured value when considering the presence of the ash layer, proving that the ash layer insulated the internal reaction layer and reduced the rate of internal heat transfer. Besides, the disparity between the internal and external temperature differences gradually amplifies with an increase in the reaction temperature. This can be attributed to the fact that the temperature reduction within the unreacted carbon core primarily relies on the reaction rate, whereas the temperature decrease in the external ash layer predominantly depends on the heat conduction of the ash layers. It can be anticipated that this dissimilarity will become more pronounced at higher gasification temperatures, consequently impacting the gasification activity.

4.4. Heat transfer analysis

The results of the reaction heat curves obtained by the thermogravimetric and differential scanning calorimetry (TG-DSC) and theoretical values calculated in this study in the gasification process of single-

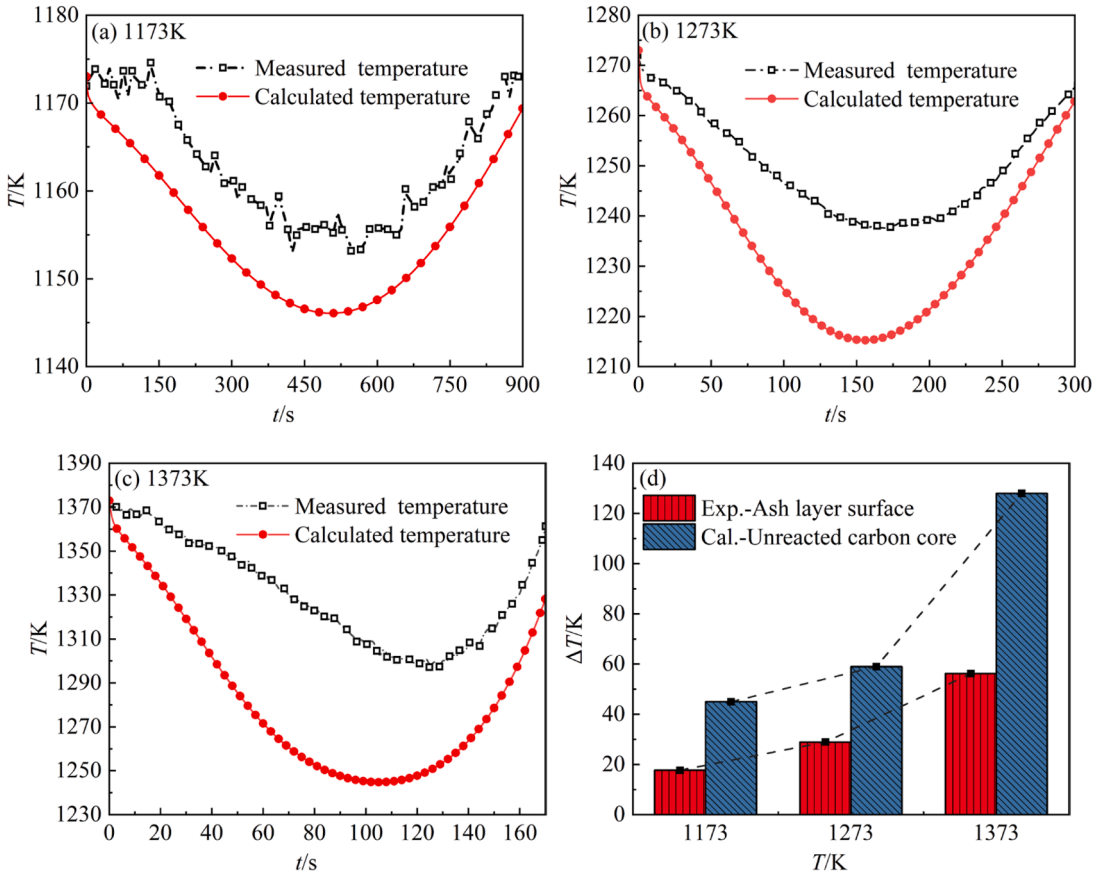

Fig. 6. The variation of measured ash layer surface temperature and unreacted carbon core temperature at different gasification temperatures (a) ~(c), and (d) the comparison of the maximum difference of the experimental ash layer surface temperature and the calculated unreacted carbon core.

particle coal char are shown in Fig. 7. The DSC curve reflects the enthalpy change of the sample, and the trend was directly related to the reactivity. The rate of reaction heat reaches the highest value rapidly in the initial stage and then decreases gradually, which is related to the gradual decrease of the reaction rate. The theoretical reaction heat curves had a high compliance value with the actual results, which proved the accuracy of the calculation of reaction heat and heat transfer in this study.

The heat transfer rates in different gasification temperatures are shown in Fig. 8, and relative time τ_t (τ_t=t_t/t_{total}) is employed here to visually show the variation in particle heat transfer at different gasification temperatures. During the reaction process, the heat conduction rate (Q_d) and the particle heat absorption rate (Q_c) showed a trend of increasing and then decreasing. The presence of the ash layer played an inhibitory role in the heat transfer of the reaction process, which is mainly manifested in the decrease of the heat conduction rate. With the gasification temperature increased, the temperature difference between the unreacted carbon core and the environment increased, and the heat transfer rate increased. Further, the heat conduction with the ash layer is approximately 1~2 orders of magnitude higher than the internal heat transfer rate, conduction is still the primary mode of heat transfer. The majority of the heat in the reaction process originated from the external environment, and the heat conduction rate directly influenced the temperature of the carbon particle surface. Meanwhile, a comparison of the results at different temperatures revealed that an increase in temperature led to an increase in the heat transfer rate.

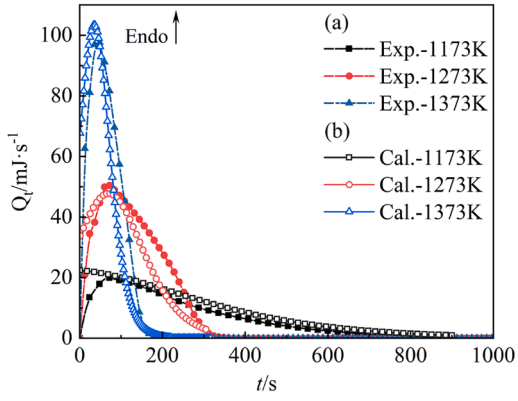

Fig. 7. Comparison of experimental results and calculated values of reaction heat curves during particle gasification process.

4.5. Kinetic model

The key parameters in the model, including the activation energy and the pre-exponential factor, are determined by fitting the data from the four mathematical models to the experimental results. The fit degree is shown in Fig. 9. Some deviations existed in the fitting results of the three conventional models for the single coal particle gasification process, especially at the initial and the late of the reaction. Specifically, the model predicted a fast reaction rate in the initial and a slow reaction rate at the end of the reaction. While, the modified kinetic model fitting results exhibited a high level of conformity with the experimental values for the reaction-driven gasification process, especially in the initial stages of the reaction.

Meanwhile, the kinetic parameters of the kinetic models, including R-squared (R^2), pre-exponential factor (k_0), and activation energy (E_a), are shown in Table 5. In the RPM model of isothermal gasification, the pore structure parameter ψ was determined by fitting the reduced time

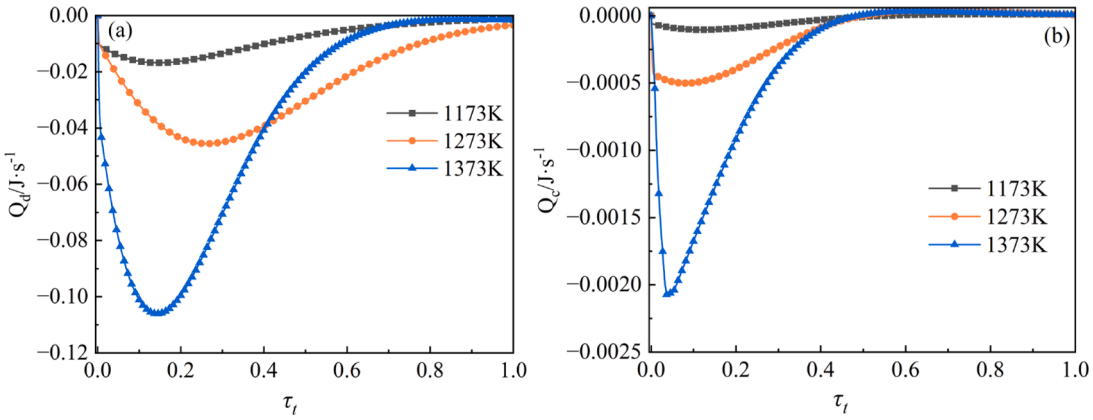

Fig. 8. Heat transfer curves versus relative time at different temperatures, (a) heat conduction, and (b) particle heat absorption.

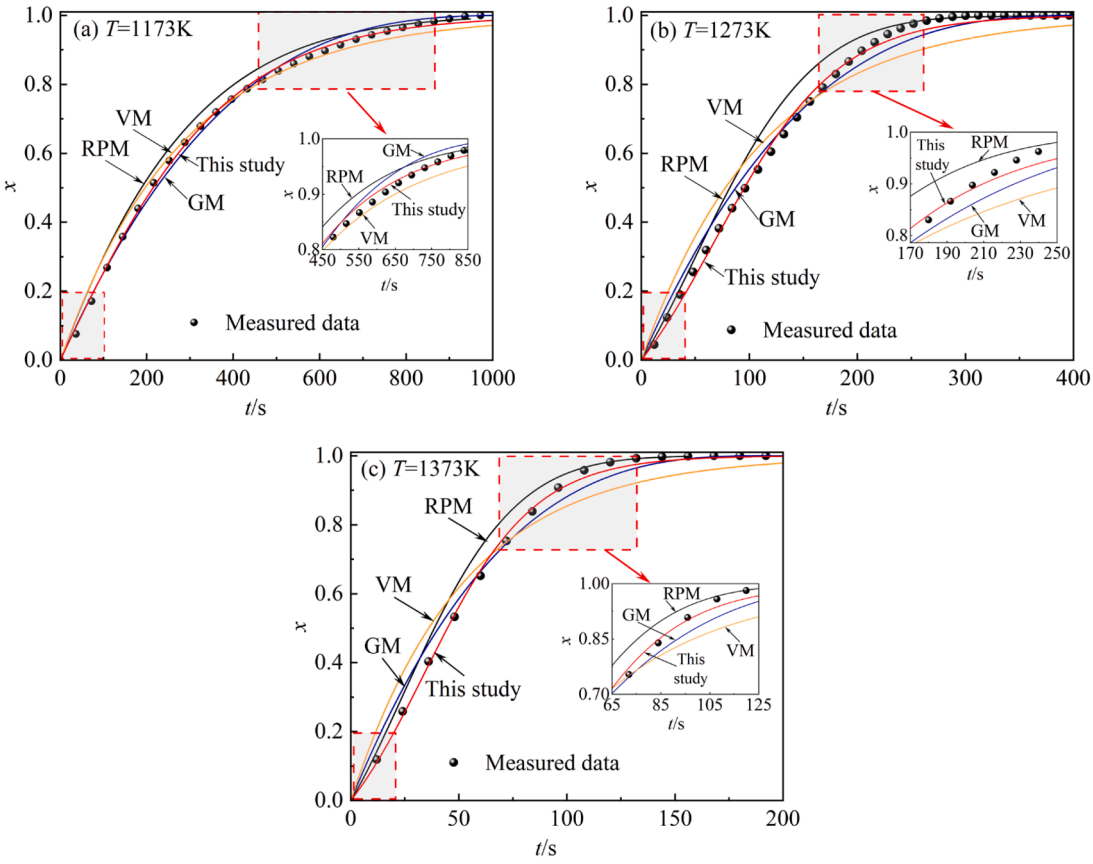

Fig. 9. Experimental data and the kinetic model fitting curves of the gasification process.

($t_x/t_{0.8}$) equation according to the experimental results obtained from TG [27], and the fitting result of the pore structure parameter ψ is 4.84. The VM and RPM models had poor fitting results compared with the other models, and this could be attributed to certain limitations in the model assumptions. VM model assumes that the gasification reaction occurred uniformly throughout the particles, whereas the RPM model assumes that the reaction occurs on the pore surface and the pores would grow or merge as the reaction proceeded. However, neither of the models accounted for the contraction of the carbon core. Conversely, the GM presented relatively favorable fitting results. This model assumes that the gasification reaction initiated from the surface of the particles and proceeded inward, maintaining a continuous contraction of the carbon particles during the gasification process, which was consistent with the assumption in this study. Compared with the above results, based on the consideration of the effect of the ash layer on the temperature and reaction area, the modified kinetic model fitting results exhibited a high level of conformity with the experimental values for the reaction-driven gasification process, and the value of R-squared (R^2) exceeded 0.998. The result also demonstrated the accuracy of the modified kinetic model in reactivity prediction for the gasification

Table 5
Kinetic parameters of different gasification models.

Parameters	RPM	GM	VM	This study
E_a (kJ/mol)	123.64	113.81	113.41	108.46
k_0 (s^{-1})	384	328	398	416
R^2	0.9742	0.9931	0.9751	0.9986

process.

The reaction activation energy and frequency factor were further calculated based on the Arrhenius equation and experimental results. The activation energy E_a represents the energy required for the molecules to reach the active state of the chemical reaction while the frequency factor k_0 represents the effective collision probability, respectively. Compared to the kinetic data in Table 5, the fitting result of the modified kinetic model has a lower activation energy than the rest, which is due to the compensation of the kinetics after considering the actual temperature of the internal carbon layer is lower by tens of degrees than particle surface temperature. k_0 is higher in the modified kinetic model, indicating that the effective collision probability is elevated and the coal gasification activity is higher than the results of the conventional reaction model.

5. Conclusion

This study employed an in-situ measurement of single coal particle gasification using a visualized temperature measurement system. The results show that the surface temperature exhibited a hierarchical distribution with a low temperature in the center of the particle during the gasification process. As the gasification temperature increased from 1173 K to 1373 K, the maximum average temperature differences increased from 17 K to 56 K. Meanwhile, affected by the differences in the active sites and particle structure, the surface temperature distribution shows inhomogeneity, with particle surface temperature difference reaching up to 80 K. Considering the presence of the ash layer, the actual reaction temperature of the internal core was calculated, and the kinetics model within the reaction process was modified. The results revealed that the temperature difference between the unreacted carbon core, and the surroundings was significantly higher than the measured results. The presence of the ash layer hindered the heat transfer. Meanwhile, a modified kinetic model was proposed based on the consideration of the unreacted core temperature and reaction area. Compared with the traditional gasification model, the model predictions demonstrated a favorable agreement with the experimental values, particularly in the initial and late stages of the reaction. This study offers novel insights into the heat transfer and reaction processes occurring during gasification, serving as a valuable reference for predicting reactivity and achieving complete conversion of coal particles.

CRediT authorship contribution statement

Haigang Zhang: Writing – review & editing, Writing – original draft, Methodology, Investigation, Formal analysis, Data curation. **Zhongjie Shen:** Writing – review & editing, Supervision, Methodology, Funding acquisition, Conceptualization. **Jianliang Xu:** Writing – original draft, Software, Methodology, Formal analysis. **Qinfeng Liang:** Writing – review & editing, Methodology, Investigation, Formal analysis. **Zhenghua Dai:** Writing – review & editing, Visualization, Validation, Supervision. **Jianhong Gong:** Writing – review & editing, Supervision, Methodology. **Haifeng Liu:** Writing – review & editing, Visualization, Validation, Supervision, Funding acquisition, Formal analysis.

Declaration of competing interest

The authors declare that they have no known competing financial interests or personal relationships that could have appeared to influence the work reported in this paper.

Data availability

The authors are unable or have chosen not to specify which data has been used.

Acknowledgments

This study is supported by the National Natural Science Foundation of China (22378130), the National Key R&D Program of China (2022YFC3902502-04), Key R&D Program of Xinjiang Uygur Autonomous Region (2022B03026-1), the Fundamental Research Funds of the Central Universities (2022ZFJH004).

Supplementary materials

Supplementary material associated with this article can be found, in the online version, at doi:10.1016/j.ijheatmasstransfer.2024.125768.

References

[1] Y. Wang, X. Bai, L. Wu, Y. Zhang, S. Qu, The petrographic compositions of Chinese commercial coals: a national survey and statistical analysis, Fuel 310 (2022) 122323.
[2] Q. Wang, X. Song, Why do China and India burn 60% of the world's coal? A decomposition analysis from a global perspective, Energy 227 (2021) 120389.
[3] T. Matamba, S. Iglauer, A. Keshavarz, A progress insight of the formation of hydrogen rich syngas from coal gasification, J. Energy Inst. 105 (2022) 81–102.
[4] Z. Shen, J. Li, H. Liu, Outlook of energy storage via large-scale entrained-flow coal gasification, Engineering 29 (2023) 50–54.
[5] M.S. Alagha, P. Szentannai, Analytical review of fluid-dynamic and thermal modeling aspects of fluidized beds for energy conversion devices, Int. J. Heat Mass Transf. 147 (2020) 118907.
[6] J. Ochoa, M.C. Cassanello, P.R. Bonelli, A.L. Cukierman, CO_2 gasification of Argentinean coal chars: a kinetic characterization, Fuel Process. Technol. 74 (2001) 161–176.
[7] F. An, F. Küster, R. Ackermann, S. Guhl, A. Richter, Heat and mass transfer analysis of a high-pressure TGA with defined gas flow for single-particle studies, Chem. Eng. J. 411 (2021) 128503.
[8] Y. Wang, Z. Gu, S. Wang, P. He, The temperature measurement technology of infrared thermal imaging and its applications review, in: 2017 13th IEEE Int. Conf. Electron. Meas. Instrum. ICEMI, 2017, pp. 401–406.
[9] H.M. Abdelmotalib, M.A.M. Youssef, A.A. Hassan, S.B. Youn, I.-T. Im, Heat transfer process in gas–solid fluidized bed combustors: a review, Int. J. Heat Mass Transf. 89 (2015) 567–575.
[10] T. Yamashita, Y. Fujii, Y. Morozumi, H. Aoki, T. Miura, Modeling of gasification and fragmentation behavior of char particles having complicated structures, Combust. Flame 146 (2006) 85–94.
[11] J. Brix, L.G. Navascués, J.B. Nielsen, P.L. Bonnek, H.E. Larsen, S. Clausen, P. Glarborg, A.D. Jensen, Oxy-fuel combustion of millimeter-sized coal char: particle temperatures and NO formation, Fuel 106 (2013) 72–78.
[12] M. Si, Q. Cheng, Q. Zhang, D. Wang, Z. Luo, C. Lou, Study of temperature, apparent spectral emissivity, and soot loading of a single burning coal particle using hyperspectral imaging technique, Combust. Flame 209 (2019) 267–277.
[13] F. Küster, P. Nikrityuk, M. Junghanns, S. Nolte, A. Tünnermann, R. Ackermann, A. Richter, S. Guhl, B. Meyer, In-situ investigation of single particle gasification in a defined gas flow applying TGA with optical measurements, Fuel 194 (2017) 544–556.
[14] S. Zhou, Z. Shen, Q. Liang, J. Xu, Z. Dai, H. Liu, Numerical simulation analysis of the induced thrust on a char particle in reaction process, AIChE J. 68 (2022).
[15] S. Yang, X. Liu, S. Wang, K. Zhang, H. Wang, Eulerian-Lagrangian simulation study of the gas-solid reacting flow in a bubbling fluidized coal gasifier, Chem. Eng. J. 426 (2021) 130825.
[16] D. Kong, K. Luo, S. Wang, J. Yu, J. Fan, Particle behaviours of biomass gasification in a bubbling fluidized bed, Chem. Eng. J. 428 (2022) 131847.
[17] A.M. Beckmann, J. Bibrzycki, M. Mancini, A. Szlęk, R. Weber, Mathematical modeling of reactants' transport and chemistry during oxidation of a millimeter-sized coal-char particle in a hot air stream, Combust. Flame 180 (2017) 2–9.
[18] C. Zou, L. Cai, C. Zheng, Numerical research on the homogeneous/heterogeneous ignition process of pulverized coal in oxy-fuel combustion, Int. J. Heat Mass Transf. 73 (2014) 207–216.
[19] S. Sładek, A. Korus, A. Klimanek, E. Karchniwy, W.P. Adamczyk, A. Szlęk, Measurements of surface temperature distributions on coal dust particles, Energy 243 (2022) 123025.
[20] R. Khatami, Y.A. Levendis, On the deduction of single coal particle combustion temperature from three-color optical pyrometry, Combust. Flame 158 (2011) 1822–1836.
[21] D.O. Glushkov, R.I. Egorov, D.M. Klepikov, High-speed contactless measurements of temperature evolution during ignition and combustion of coal-based fuel pellets, Int. J. Heat Mass Transf. 175 (2021) 121359.
[22] M.A. Kibria, P. Sripada, M.W. Woo, S. Bhattacharya, Fate of a biomass particle during CO2 gasification: a mathematical model under entrained flow condition at high temperature, Energy 168 (2019) 1045–1062.
[23] A. Ramos, E. Monteiro, A. Rouboa, Numerical approaches and comprehensive models for gasification process: a review, Renew. Sustain. Energy Rev. 110 (2019) 188–206.
[24] M.F. Irfan, M.R. Usman, K. Kusakabe, Coal gasification in CO2 atmosphere and its kinetics since 1948: a brief review, Energy 36 (2011) 12–40.

[25] M. Liu, Q. He, J. Bai, J. Yu, L. Kong, Z. Bai, H. Li, C. He, X. Cao, Z. Ge, W. Li, Char reactivity and kinetics based on the dynamic char structure during gasification by CO2, Fuel Process. Technol. 211 (2021) 106583.
[26] K. Bikane, J. Yu, R. Shankar, X. Long, N. Paterson, M. Millan, Early-stage kinetics and char structural evolution during CO2 gasification of Morupule coal in a wire-mesh reactor, Chem. Eng. J. 421 (2021) 127803.
[27] X. Gao, Y. Zhang, B. Li, Y. Zhao, B. Jiang, Determination of the intrinsic reactivities for carbon dioxide gasification of rice husk chars through using random pore model, Bioresour. Technol. 218 (2016) 1073–1081.
[28] K.M. Steel, R.E. Dawson, D.R. Jenkins, R. Pearce, M.R. Mahoney, Use of rheometry and micro-CT analysis to understand pore structure development in coke, Fuel Process. Technol. 155 (2017) 106–113.
[29] Q. He, Y. Gong, L. Ding, Q. Guo, K. Yoshikawa, G. Yu, Reactivity prediction and mechanism analysis of raw and demineralized coal char gasification, Energy 229 (2021) 120724.
[30] K. Wang, Y. Wang, H. Guo, J. Zhang, G. Zhang, Modeling of multiple gas transport mechanisms through coal particle considering thermal effects, Fuel 295 (2021) 120587.
[31] R. Gupta, Advanced coal characterization: a review, Energy Fuels 21 (2007) 451–460.
[32] L. Ding, Y. Gong, Y. Wang, F. Wang, G. Yu, Characterisation of the morphological changes and interactions in char, slag and ash during CO_2 gasification of rice straw and lignite, Appl. Energy 195 (2017) 713–724.
[33] H. Zhang, Z. Shen, J. Xu, Q. Liang, Z. Dai, H. Liu, New insight to migration and influence of potassium element on combustion of coal/biomass char-slag interface, Combust. Flame 257 (2023) 112969.
[34] E.G. Pereira, J.N. da Silva, J.L. de Oliveira, C.S. Machado, Sustainable energy: a review of gasification technologies, Renew. Sustain. Energy Rev. 16 (2012) 4753–4762.
[35] F. Jiao, K. Wang, F. Shuang, D. Dong, L. Jiao, A smartphone-based sensor with an uncooled infrared thermal camera for accurate temperature measurement of pig groups, Front. Phys. 10 (2022) 893131.
[36] Z. Song, X. Huang, M. Luo, J. Gong, X. Pan, Experimental study on the diffusion–kinetics interaction in heterogeneous reaction of coal, J. Therm. Anal. Calorim. 129 (2017) 1625–1637.
[37] P.N. Sharratt, R. Mann, Some observations on the variation of tortuosity with Thiele modulus and pore size distribution, Chem. Eng. Sci. 42 (1987) 1565–1576.
[38] Z. Shen, Q. Liang, J. Xu, B. Zhang, D. Han, H. Liu, In situ experimental study on the combustion characteristics of captured chars on the molten slag surface, Combust. Flame 166 (2016) 333–342.
[39] Y.T. Kim, D.K. Seo, J. Hwang, Study of the effect of coal type and particle size on char–CO_2 gasification via gas analysis, Energy Fuels 25 (2011) 5044–5054.
[40] G. Soon, H. Zhang, A.W.-K. Law, C. Yang, Computational modelling on gasification processes of municipal solid wastes including molten slag, Waste 1 (2023) 370–388.
[41] G.H. Fong, S. Jorgensen, S.L. Singer, Pore-resolving simulation of char particle gasification using micro-CT, Fuel 224 (2018) 752–763.
[42] Z. Shen, J. Xu, H. Liu, Q. Liang, Modeling study for the effect of particle size on char gasification with CO_2, AIChE J 63 (2017) 716–724.